Goedert, M., 2000. -synuclein and neurodegenerative diseases. Nat. Rev. Neurosci. 2, 492–501.
Hardy, J., Gwinn-Hardy, K., 1998. Genetic classification of primary neurodegenerative disease. Science 282, 1075–1079.
Hasegawa, M., Fujiwara, H., Nonaka, T., Wakabayashi, K., Takahashi, H., Lee, V.M., Trojanowski, J.Q., Mann, D., Iwatsubo, T., 2002. Phosphorylated α-synuclein is ubiquitinated in alpha-synucleinopathy lesions. J. Biol. Chem. 277, 49071–49076.
Ikarashi, Y., Harigaya, Y., Tomidokoro, Y., Kanai, M., Ikeda, M., Matsubara, E., Kawarabayashi, T., Kuribara, H., Younkin, S.G., Maruyama, Y., Shoji, M., 2004. Decreased level of brain acetylcholine and memory disturbance in APPsw mice. Neurobiol. Aging 25, 483–490.
Ikarashi, Y., Sasahara, T., Maruyama, Y., 1985. Postmortem changes in catecholamines, indoleamines, and their metabolites in rat brain regions: prevention with 10-kW microwave irradiation. J. Neurochem. 45, 935–939.
Ikarashi, Y., Blank, C.L., Maruyama, Y., 1992. Glassy carbon pre-column for determination of acetylcholine and choline in biological samples using liquid chromatography with electrochemical detection. J. Chromatogr. 575, 29–37.
Ikeda, M., Shoji, M., Kawarai, T., Kawarabayashi, T., Matsubara, E., Murakami, T., Sasaki, A., Tomidokoro, Y., Ikarashi, Y., Kuribara, H., Ishiguro, K., Hasegawa, M., Yen, S.H., Chishti, M.A., Harigaya, Y., Abe, K., Okamoto, K., St George-Hyslop, P., Westaway, D., 2005. Accumulation of filamentous tau in the cerebral cortex of human tau R406W transgenic mice. Am. J. Pathol. 166, 521–531.
Imai, E., Akagi, Y., Isaka, Y., Ikawa, M., Takenaka, M., Hori, M., Okabe, M., 1999. Glowing podocytes in living mouse: transgenic mouse carrying a podocyte-specific promoter. Exp. Nephrol. 7, 63–66.
Iwai, A., Masliah, E., Yoshimoto, M., Ge, N., Flanagan, L., de Silva, H. A., Kittel, A., Saitoh, T., 1995. The precursor protein of non-Aβ component of Alzheimer's disease amyloid is a presynaptic protein of the central nervous system. Neuron 14, 467–475.
Iwatsubo, T., Yamaguchi, H., Fujimuro, M., Yokosawa, H., Ihara, Y., Trojanowski, J.Q., Lee, V.M., 1996. Purification and characterization of Lewy bodies from the brains of patients with diffuse Lewy body disease. Am. J. Pathol. 148, 1517–1529.
Kahle, P.J., Neumann, M., Ozmen, L., Muller, V., Jacobsen, H., Schindzielorz, A., Okochi, M., Leimer, U., van der Putten, H., Probst, A., Kremmer, E., Kretzschmar, H.A., Haass, C., 2000. Subcellular localization of wild-type and Parkinson's disease-associated mutant α-synuclein in human and transgenic mouse brain. J. Neurosci. 20, 6365–6373.
Kitada, T., Asakawa, S., Hattori, N., Matsumine, H., Yamamura, Y., Minoshima, S., Yokochi, M., Mizuno, Y., Shimizu, N., 1998. Mutations in the parkin gene cause autosomal recessive juvenile parkinsonism. Nature 392, 605–608.
Kruger, R., Kuhn, W., Muller, T., Woitalla, D., Graeber, M., Kosel, S., Przuntek, H., Epplen, J.T., Schols, L., Riess, O., 1998. Ala30Pro mutation in the gene encoding α-synuclein in Parkinson's disease. Nat. Genet. 18, 106–108.
Kuribara, H., Higuchi, Y., Tadokoro, S., 1977. Effects of central depressants on rota-rod and traction performances in mice. Jpn. J. Pharmacol. 27, 117–126.
Lee, M.K., Stirling, W., Xu, Y., Xu, X., Qui, D., Mandir, A.S., Dawson, T.M., Copeland, N.G., Jenkins, N.A., Price, D.L., 2002. Human α-synuclein-harboring familial Parkinson's disease-linked Ala-53. Thr mutation causes neurodegenerative disease with α-synuclein aggregation in transgenic mice. Proc. Natl. Acad. Sci. U. S. A. 99, 8968–8973.
Liscovitch, M., Czarny, M., Fiucci, G., Tang, X., 2000. Phospholipase D: molecular and cell biology of a novel gene family. Biochem. J. 345, 401–415.
Lotharius, J., Brundin, P., 2000. Pathogenesis of Parkinson's disease: dopamine, vesicles and α-synuclein. Nat. Rev. Neurosci. 3, 932–942.
Lowry, O.H., Rosebrough, N.J., Farr, A.L., Randall, R.J., 1951. Protein measurement with the Folin phenol reagent. J. Biol. Chem. 193, 265–275.
Masliah, E., Rockenstein, E., Veinbergs, I., Mallory, M., Hashimoto, M., Takeda, A., Sagara, Y., Sisk, A., Mucke, L., 2000. L-DOPAminergic loss and inclusion body formation in α-synuclein mice: implications for neurodegenerative disorders. Science 287, 1265–1269.
Murakami, T., Paitel, E., Kawarabayashi, T., Ikedame>M., Chishti, M.A., Janus, C., Matsubara, E., Sasaki, A., Kawarai, T., Phinney, A.L., Harigaya, Y., Horne, P., Egashira, N., Mishima, K., Hanna, A., Yang, J., Iwasaki, K., Takahashi, M., Fujiwara, M., Ishiguro, K., Bergeron, C., Carlson, G.A., Abe, K., Westaway, D., St. George-Hyslop, P., Shoji, M., 2006. Cortical neuronal and glial pathology in TgTauP301L transgenic mice: neuronal degeneration, memory disturbance, and phenotypic variation. Am. J. Pathol. 169, 1343–1352.
Neumann, M., Kahle, P.J., Giasson, B.I., Ozmen, L., Borroni, E., Spooren, W., Muller, V., Odoy, S., Fujiwara, H., Hasegawa, M., 2002. Misfolded proteinase K-resistant hyperphosphorylated α-synuclein in aged transgenic mice with locomotor deterioration and in human α-synucleinopathies. J. Clin. Invest. 110, 1429–1439.
Payton, J.E., Perrin, R.J., Woods, W.S., George, J.M., 2000. Structural determinants of PLD2 inhibition by α-synuclein. J. Mol. Biol. 337, 1001–1009.
Polymeropoulos, M.H., Lavedan, C., Leroy, E., Ide, S.E., Dehejia, A., Dutra, A., Pike, B., Root, H., Rubenstein, J., Boyer, R., Stenroos, E.S., Chandrasekharappa, S., Athanassiadou, A., Papapetropoulos, T., Johnson, W.G., Lazzarini, A.M., Duvoisin, R.C., Di Iorio, G., Golbe, L.I., Nussbaum, R.L., 1997. Mutation in the α-synuclein gene identified in families with Parkinson's disease. Science 276, 2045–2047.
Richfield, E.K., Thiruchelvam, M.J., Cory-Slechta, D.A., Wuertzer, C., Gainetdinov, R.R., Caron, M.G., Di Monte, D.A., Federoff, H.J., 2002. Behavioral and neurochemical effects of wild-type and mutated human alpha-synuclein in transgenic mice. Exp. Neurol. 175, 35–48.
Sampathu, D.M., Giasson, B.I., Pawlyk, A.C., Trojanowski, J.Q., Lee, V.M., 2003. Ubiquitination of α-synuclein is not required for formation of pathological inclusions in α-synucleinopathies. Am. J. Pathol. 163, 91–100.
Shimura, H., Schlossmacher, M.G., Hattori, N., Frosch, M.P., Trockenbacher, A., Schneider, R., Mizuno, Y., Kosik, K.S., Selkoe, D.J., 2001. Ubiquitination of a new form of α-synuclein by parkin from human brain: implications for Parkinson's disease. Science 293, 263–269.
Shoji, M., Harigaya, Y., Sasaki, A., Ueda, K., Ishiguro, K., Matsubara, E., Watanabe, M., Ikeda, M., Kanai, M., Tomidokoro, Y., Shizuka, M., Amari, M., Kosaka, K., Nakazato, Y., Okamoto, K., Hirai, S., 2000. Accumulation of NACP/α-synuclein in Lewy body disease and multiple system atrophy. J. Neurol. Neurosurg. Psychiatry 68, 605–608.
Singleton, A.B., Farrer, M., Johnson, J., Singleton, A., Hague, S., Kachergus, J., Hulihan, M., Peuralinna, T., Dutra, A., Nussbaum, R., Lincoln, S., Crawley, A., Hanson, M., Maraganore, D., Adler, C., Cookson, M.R., Muenter, M., Baptista, M., Miller, D., Blancato, J., Hardy, J., Gwinn-Hardy, K., 2002. -Synuclein locus triplication causes Parkinson's disease. Science 302, 841.
Spillantini, M.G., Schmidt, M.L., Lee, V.M., Trojanowski, J.Q., Jakes, R., Goedert, M., 1997. -synuclein in Lewy bodies. Nature 388, 839–840.
Thiruchelvam, M.J., Powers, J.M., Cory-Slechta, D.A., Richfield, E.K., 2004. Risk factors for dopaminergic neuron loss in human α-synuclein transgenic mice. Eur. J. Neurosci. 19, 845–854.
Tofaris, G.K., Reitböck, P.G., Humby, T., Lambourne, S.L., O'Connell, M., Ghetti, B., Gossage, H., Emson, P.C., Wilkinson, L.S., Goedert, M., Spillantini, M.G., 2006. Pathological changes in dopaminergic nerve cells of the substantia nigra and olfactory bulb in mice transgenic for truncated human

α-synuclein(1–120): implications for Lewy body disorders. J. Neurosci. 26, 3942–3950.

Tu, P.H., Galvin, J.E., Baba, M., Giasson, B., Tomita, T., Leight, S., Nakajo, S., Iwatsubo, T., Trojanowski, J.Q., Lee, V.M., 1998. Glial cytoplasmic inclusions in white matter oligodendrocytes of multiple system atrophy brains contain insoluble α-synuclein. Ann. Neurol. 44, 415–422.

Ueda, K., Fukushima, H., Masliah, E., Xia, Y., Iwai, A., Yoshimoto, M., Otero, D.A., Kondo, J., Ihara, Y., Saitoh, T., 1992. Molecular cloning of cDNA encoding an unrecognized component of amyloid in Alzheimer disease. Proc. Natl. Acad. Sci. U. S. A. 90, 11282–11286.

van der Putten, H., Wiederhold, K.H., Probst, A., Barbieri, S., Mistl, C., Danner, S., Kauffmann, S., Hofele, K., Spooren, W.P., Ruegg, M.A., Lin, S., Caroni, P., Sommer, B., Tolnay, M., Bilbe, G., 2000. Neuropathology in mice expressing human α-synuclein. J. Neurosci. 20, 6021–6029.

Wakamatsu, M., Ishii, A., Ukai, Y., Sakagami, J., Iwata, S., Ono, M., Matsumoto, K., Nakamura, A., Tada, N., Kobayashi, K., Iwatsubo, T., Yoshimoto, M., 2007. Accumulation of phosphorylated α-synuclein in dopaminergic neurons of transgenic mice that express human α-synuclein J. Neurosci. Res. 85, 1819–1825.

Wakamatsu, M., Ishii, A., Iwata, S., Sakagami, J., Ukai, Y., Ono, M., Kanbe, D., Muramatsu, S., Kobayashi, K., Iwatsubo, T., Yoshimoto, M., 2008. Selective loss of nigral dopamine neurons induced by overexpression of truncated human α-synuclein in mice. Neurobiol. Aging 29, 574–585.

Zarranz, J.J., Alegre, J., Gomez-Esteban, J.C., Lezcano, E., Ros, R., Ampuero, I., Vidal, L., Hoenicka, J., Rodriguez, O., Atares, B., Llorens, V., Gomez Tortosa, E., del Ser, T., Munoz, D.G., de Yebenes, J.G., 2004. The new mutation, E46K, of α-synuclein causes Parkinson and Lewy body dementia. Ann. Neurol. 55, 164–173.

ABSTRACT: β-Synemin was previously identified as an α-dystrobrevin–interacting protein in muscle. To better understand its function in neural tissue, in situ and immunohistochemical analyses were performed to identify where the synemin isoforms are expressed in the spinal cord of C57BL/6 and dystrophin-deficient (*mdx*) C57BL/10 mice. These analyses show that synemin transcript and its encoded protein colocalize in the anterior horn cells and that no differences in synemin expression were found in nerve tissue from C57BL/6 or *mdx* mice. The expression of synemin mRNA and protein predominantly in the anterior horn cells suggests that synemin performs an essential function in those cells. Because synemin is more highly expressed in the midbrain and pons, its function in neurological cells was further pursued by identifying coexpressed proteins in cells from those regions of the brain. These results show that neurons that express synemin also express tryptophan hydroxylase-1, a marker of serotoninergic nerve fibers.

Muscle Nerve **39:** 634–641, 2009

EXPRESSION OF SYNEMIN IN THE MOUSE SPINAL CORD

YUJI MIZUNO, MD, PhD,[1] JEFFREY R. GUYON, PhD,[2] KOICHI OKAMOTO, MD, PhD,[1] and LOUIS M. KUNKEL, PhD[2]

[1] Department of Neurology, Gunma University Graduate School of Medicine, 3-39-22 Showa, Maebashi, Gunma 371-8511, Japan
[2] Howard Hughes Medical Institute/Division of Genetics, Children's Hospital Boston and Harvard Medical School, Boston, Massachusetts, USA

Accepted 6 October 2008

Synemin is a type VI member of the intermediate filament (IF) protein superfamily.[16] IF proteins are composed of three common structural regions, including the N-terminus head domain, the central α-helical rod domain, and the C-terminus tail domain. Among type VI IF proteins, synemin is unique in that it has a very short N-terminus and a long C-terminus,[13] thus the C-terminus may be important for protein–protein interactions.

In mammals, there are two synemin isoforms (α and β), whereas only one synemin isoform is expressed in birds. The mammalian α-synemin[28,32] mRNA is structurally identical[16,28] to β-synemin (also called desmuslin),[16] with the exception that intron 4 of β-synemin is not spliced from the α-synemin transcript. This difference results in an additional α-synemin coding region, which is 906 bp long in mice[32] and 936 bp long in humans.[16] Although the function of α-synemin is unknown, it is expressed predominantly in brain tissue, whereas β-synemin is strongly expressed in skeletal and cardiac muscle.

In muscle, the synemin protein forms heteropolymeric IFs with desmin and vimentin,[7] which are two different type III IF proteins. Desmin and vimentin encircle and connect the myofibrillar Z-lines of the neighboring myofibrils, and they also bind the Z-lines of myofibrils to the sarcolemma at the costamere. In addition, β-synemin was originally identified as an α-dystrobrevin–binding protein through a yeast two-hybrid screen.[16] Although β-synemin can theoretically bind either α-dystrobrevin-1 or -2,[16] it is thought that β-synemin preferentially associates with α-dystrobrevin-1 in skeletal muscle.[14] There is considerable evidence for this association. For example, it has been shown that α-dystrobrevin-1 (rather than α-dystrobrevin-2) preferentially co-immunoprecipitates with β-synemin in rat skeletal muscle.[12] β-Synemin and α-dystrobrevin-1 are expressed at the same developmental time (in mice, 5 days post-birth), whereas α-dystrobrevin-2 is detectable before birth.[12] β-Synemin and α-dystrobrevin-1 are expressed at the

Abbreviations: CNS, central nerve system; EDTA, ethylene-diamine tetraacetic acid; IF, intermediate filament, PBS, phosphate-buffered saline; TBS, Tris-buffered saline; TBST, Tween-20 plus Tris-buffered saline; TPH-1, tryptophan hydroxylase-1

Key words: α-dystrobrevin; anterior horn cell; spinal cord; synemin; tryptophan hydroxylase

Correspondence to: Y. Mizuno; e-mail: mizunoy@med.gunma-u.ac.jp

Published online 21 January 2009 in Wiley InterScience (www.interscience.wiley.com). DOI 10.1002/mus.21221

same time in regenerating adult muscle (day 7 following cardiotoxin injection), whereas α-dystrobrevin-2 is observed as early as day 1 post-injection.[12] α-Dystrobrevin-1 and β-synemin expression levels are similar between control and dystrophin-deficient (*mdx*) mouse skeletal muscle, whereas α-dystrobrevin-2 expression is greatly decreased in *mdx* mice.[14] Taken together, these data suggest that β-synemin participates in the stabilization of muscle by linking the myofibrillar Z-lines with the membrane-associated α-dystrobrevin-1 protein at the costameres.

This role for synemin in muscle is further strengthened by its interactions with other muscle proteins. For example, birds express only one synemin isoform (α-synemin), which has been shown to bind α-actinin (an actin-binding protein) and vinculin (a costameric protein).[1] Recent studies have also shown that human α-synemin interacts directly with both vinculin and metavinculin.[26] Human β-synemin was originally identified as an α-dystrobrevin–interacting protein[16] and α-dystrobrevin is a known member of the dystrophin-associated protein complex.[21–23] The association with dystrophin is also strengthened by recent evidence that has shown avian synemin binds directly to dystophin and utrophin (a dystrophin homologue).[3] Given that synemin interacts with a number of different muscle structural proteins and is present at adhesion-type junctions, such as costameres,[3] these findings suggest that synemin likely functions in maintaining cell structural integrity and stabilizing the cytoskeleton in muscle cells during repeated cycles of cell relaxation and contraction.

In addition to muscle, synemin isoforms are also expressed in other tissues. For example, additional in situ hybridization and immunohistochemical experiments confirmed that the synemin transcript was translated into protein in neurons located in regions of the dorsal side of the midbrain and pons.[13] Using an isoform-specific synemin RNA in situ probe, it has been shown that the α-synemin isoform is expressed in these same neurons.[13] The finding that synemin is expressed in such a limited subset of nerve cells suggests that this gene plays a specific role in neuronal tissue, which is likely much different than that performed in skeletal muscle.

Given that synemin is expressed in specific neurons within the brain, it seemed likely that this protein would also be expressed in the spinal cord, a region central to many debilitating human neurological diseases. Izmiryan et al. suggested that synemin was not highly expressed in the adult mouse spinal cord.[8] Because their findings[8] were based on an immunohistochemical analysis, this analysis was repeated using both RNA-based (in situ hybridization) and additional protein-based (immunohistochemistry) approaches to reanalyze if the synemin transcript and protein are expressed in the spinal cord. Because β-synemin is strongly expressed in muscle and has been shown to interact with dystrophin in vitro,[3] synemin expression in spinal cord from 8-week-old control C57BL/6 mice and dystrophin-deficient C57BL/10 mice was also examined. Sections were analyzed using a synemin RNA probe with homology to a non-coding region common to both synemin isoforms, and a human anti-synemin antibody that recognizes both the α- and β-synemin proteins. Because these findings showed that synemin was only weakly expressed in the spinal cord, we returned to brain to better characterize synemin-expressing neurons in the midbrain and pons. Our results in brain show that synemin is coexpressed with tryptophan hydroxylase-1, a marker of serotoninergic nerve cells.

METHODS

RNA Probe Design and Preparation. The in situ probe used was synemin RNA probe-3 [479-bp; position 5972–6450 (5907–6385 bp from the initiation codon)]. The position designation is relative to the mouse muscle cDNA for synemin (GenBank Accession No. NM_201639). This probe was created by subcloning the synemin fragment into a pGEM-T vector (Promega, Madison, Wisconsin) and generating digoxigenin-RNA sense and anti-sense probes from the flanking T7 and S6 promoters (Roche, Basel, Switzerland).

In Situ Hybridization. All in situ hybridization protocols were performed by Genostaff, Inc. (Tokyo, Japan), and all results were confirmed through multiple replications. Mouse brain was isolated from both 8-week-old C57BL/6 and dystrophin-deficient (*mdx*) C57BL/10 mice, fixed with tissue fixative, and embedded in paraffin blocks. Dystrophic (*mdx*) mice were provided by the Central Institute for Experimental Animals (Kanagawa, Japan). Tissue sections (6 μm) were prepared for in situ hybridization by de-waxing with xylene and rehydrating through a series of washes with ethanol and phosphate-buffered saline (PBS). Sections were fixed in PBS with 4% paraformaldehyde for 15 min and then washed with PBS. Sections were then treated with 10 μg/ml proteinase K in PBS for 30 min at 37°C, washed with PBS, refixed with 4% paraformaldehyde in PBS, washed again with PBS, and placed in 0.2 M HCl for 10 min.

After washing with PBS, sections were acetylated by incubation in 0.1 M triethanolamine–HCl (pH 8.0) plus 0.25% acetic anhydride for 10 min. Sections were then washed with PBS and dehydrated through a series of ethanol washes. Hybridization was performed with RNA probe-3 (100 ng/ml) in probe diluent at 60°C for 16 h. After hybridization, sections were washed in 5 × HybriWash (Genostaff) at 60°C for 20 min and then in 50% formamide, 2 × HybriWash at 60°C for 20 min, followed by RNase treatment in 50 μg/ml RNaseA in 10 mM Tris-HCl (pH 8.0), 1 M NaCl, and 1 mM ethylene-diamine tetraacetic acid (EDTA) for 30 min at 37°C. The sections were then washed twice with 2 × HybriWash at 60°C for 20 min, twice with 0.2 × HybriWash at 60&deh;C for 20 min, and once with TBST [0.1% Tween-20 in Tris-buffered saline (TBS)]. After treatment with 0.5% blocking reagent (Roche, Basel, Switzerland) in TBST for 30 min, sections were incubated with anti-digoxigenin–AP conjugate (Roche) diluted 1:1000 with TBST for 2 h. The sections were washed twice with TBST and incubated in 100 mM NaCl, 50 mM $MgCl_2$, 0.1% Tween-20, and 100 mM Tris-HCl (pH 9.5). Coloring reactions were performed with BM purple AP substrate (Roche) overnight and washed with PBS. The sections were counterstained with Kernechtrot stain solution (Muto Pure Chemicals, Tokyo, Japan), dehydrated, and mounted with malinol (Muto Pure Chemicals).

Immunohistochemistry. For immunohistochemistry, tissue sections were de-waxed with xylene, and rehydrated through a series of ethanol and TBS washes. Antigen retrieval was performed by microwaving the samples for 20 min with citrate buffer (pH 6.0). The sections were treated with 3% hydrogen peroxide in methanol for 30 min, and protein block (Dako, Kyoto, Japan) for 10 min. The sections were treated with anti-human synemin rabbit polyclonal antibody[15–17] at a final concentration of 0.4 μg/ml at 2°–8°C overnight or anti–tryptophan hydroxylase-1 (anti–TPH-1) rabbit monoclonal antibody (Epitomics, Burlingame, California) at a final concentration of 2 μg/ml at 4°C overnight. The 12-amino acid peptide sequence used to generate the anti-human synemin antibody is conserved in mice (amino acids 857–868 in human[13] and 848–859 in mouse[32]). For synemin staining, sections were treated with Histofine Simplestain Mouse MAX-PO (R) (Nichirei Biosciences, Tokyo, Japan) for 30 min and incubated with 3,3′-diaminobenzidine tetrahydrochloride (Wako Pure Chemical Industries, Osaka, Japan). For TPH-1 staining, sections were treated with a biotin-blocking system (Dako) and successively incubated with biotinylated anti-rabbit immunoglobulins (Dako) diluted 1:600 for 30 min, peroxidase-conjugated streptavidin (Nichirei Biosciences) for 5 min, and 3,3′-diaminobenzidine tetrahydrochloride (Wako Pure Chemical Industries). Sections were counterstained with Mayer's hematoxylin (Muto Pure Chemicals), dehydrated, and mounted with malinol (Muto Pure Chemicals). To better highlight signal differences, digital pictures taken under identical light conditions were modified together as a group by making a minor adjustment to the contrast level in Photoshop (Adobe Systems, Inc., San Jose, California).

RESULTS

Localization of Synemin Transcript and Its Protein in Spinal Cord in Sagittal Sections. To investigate synemin expression in the mouse spinal cord, in situ analysis was performed on sagittal sections using the general synemin probe-3. Positive structures were visible on the ventral side of the spinal cord, but it was hard to discriminate individual neurons expressing synemin transcript when they were viewed at low magnification (Fig. 1A). Higher magnification of the ventral side showed more obvious staining of synemin transcript (Fig. 1C), and even further magnification of the area in Figure 1C makes it possible to clearly discern individual reactive neurons (Fig. 1E). Mirror sections were used to determine colocalization of the synemin transcript and protein as a means of showing probe specificity. Immunohistochemical analysis using an antibody derived against human synemin showed ventral alignment of synemin-positive neurons (Fig. 1B). At high magnification, comparisons of the in situ and immunohistochemical analyses confirmed colocalization of the synemin transcript (Fig. 1C and E) and protein (Fig. 1D and F). Additional control experiments using sense probes were negative (data not shown). This suggests that the labeling patterns for the anti-sense probes were specific.

The synemin protein was initially identified as a α-dystrobrevin–interacting protein in muscle. To determine whether synemin expression was altered in nerve cells of a dystrophin-deficient (*mdx*) mouse, in situ hybridization and immunohistochemical experiments were performed simultaneously on control and *mdx* mouse spinal cord sections. Synemin staining intensities from the in situ hybridization (Fig. 1G and I) and immunohistochemical experiments (Fig. 1H and J) in *mdx* mice were similar to that of control mice, thus the dystrophic condition of the *mdx* mouse had no measurable effect on synemin expression in the spinal cord nerve cells.

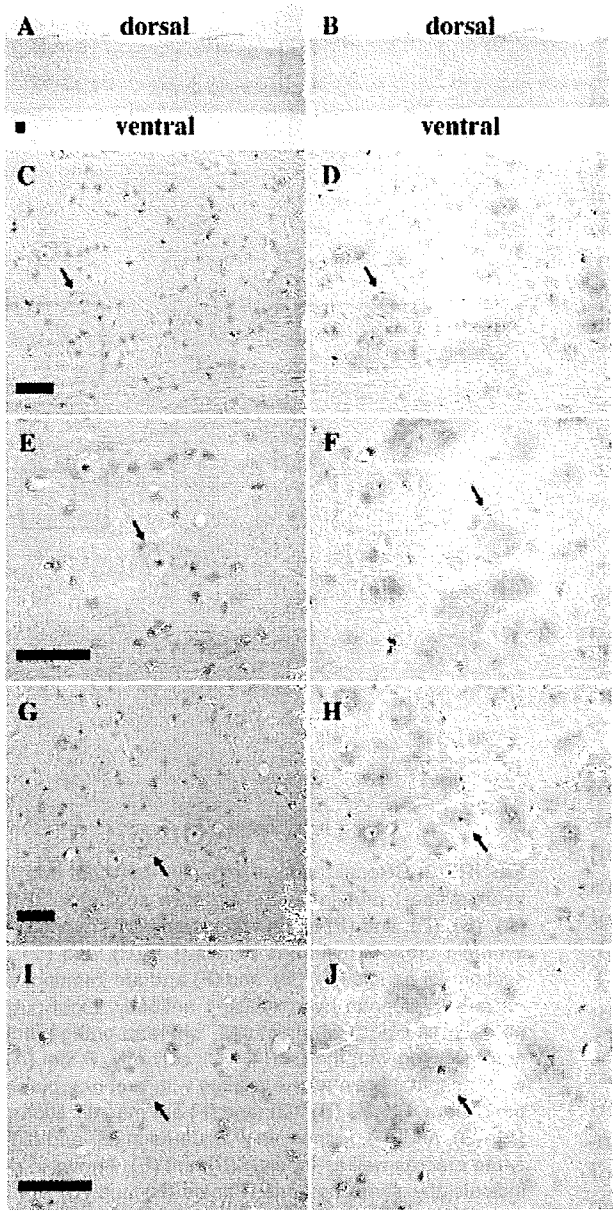

FIGURE 1. Colocalization of the synemin transcript and protein in mouse spinal cord on sagittal sections. Panels **(A)**, **(C)**, **(E)**, **(G)**, and **(I)** are in situ experiments hybridized with the synemin probe-3, whereas panels **(B)**, **(D)**, **(F)**, **(H)**, and **(J)** are mirror sections immunostained with an anti-synemin antibody. Panels **(A)–(F)** are from control mice, whereas panels **(G)–(J)** are from *mdx* mice. Light purple shows in situ–positive structures and orange indicates those immunostained with the antibody. Signals with probe-3 in **(A)** are not clearly detectable, whereas immunohistochemically positive structures seem to be more pronounced toward the ventral side of **(B)**. Panels **(C)** and **(D)** are magnified images of the same ventral side shown in panels **(A)** and **(B)**, respectively. The signals of synemin transcript seen in panel **(C)** are weak, but they are clearly visible with increased magnification **(E)**. Immunohistochemical analysis shows a clear colocalization of synemin protein, as seen in **(D)** and **(F)**. In the *mdx* mouse spinal cord, the same synemin staining patterns are seen at the same magnifications as seen in **(G)–(J)**. Arrows designate the anterior horn cells. Bar = 50 μm.

Localization of Synemin Transcript and Its Protein in Spinal Cord Using Transverse Sections. In situ hybridization and immunohistochemical analyses were performed on spinal cord transverse sections to better localize synemin expression. In situ hybridization experiments were performed under conditions similar to those described for the sagittal sections (Fig. 2A). Detailed examination of the region shown in the square in Figure 2A highlights staining of individual anterior horn cells (Fig. 2C). Further magnification of this region showed weak and irregular synemin signals in the cytoplasm of these neurons (Fig. 2E). In contrast to synemin staining in the midbrain and pons, the intensity of synemin staining in the spinal cord was relatively weak, suggesting that synemin is only expressed at low levels in these cells.

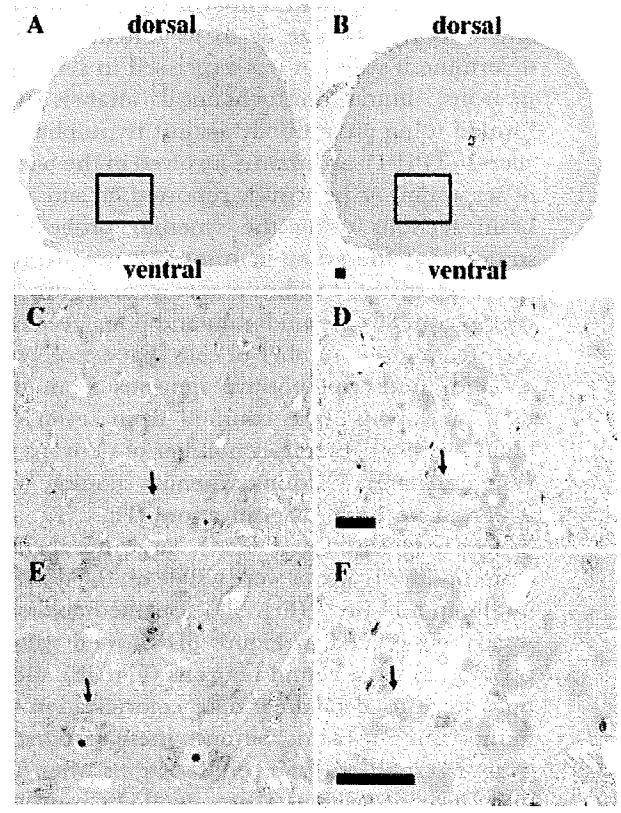

FIGURE 2. Colocalization of synemin transcript and protein in mouse spinal cord on transverse sections. Panels **(A)**, **(C)**, and **(E)** are in situ experiments hybridized with the synemin probe-3, whereas panels **(B)**, **(D)**, and **(F)** are mirror sections immunostained with an anti-synemin antibody. Light purple is indicative of in situ–positive structures, whereas orange indicates immunostained structures. The squares shown in panels **(A)** and **(B)** are magnified and shown in **(C)** and **(D)** to more clearly see the transcript-positive and protein-positive structures. Panels **(E)** and **(F)** are further magnifications of panels **(C)–(D)** to better highlight synemin. The single arrow in panels **(C)–(F)** denotes the same neurons. Bar = 50 μm.

Control experiments with synemin sense probes were negative (data not shown), suggesting that the labeling patterns for the anti-sense probes were specific. To determine whether synemin transcript and protein were expressed in the same neurons, mirror sections were examined using an anti-synemin antibody. The same anterior horn cells that expressed synemin transcript (Fig. 2C and E) also stained positively for the synemin protein (Fig. 2D and F). Synemin-positive cells were widely distributed in the lateral and posterior horns of the transverse section (Fig. 2B).

Localization of Synemin Transcript and Tryptophan Hydroxylase-1. Because synemin was only weakly expressed in the mouse spinal cord, its function was further investigated in the brain, where it is more highly expressed. By identifying coexpressed proteins, one can begin to identify neurons that express synemin and thus hypothesize as to its function in vivo. To determine if synemin was expressed in serotoninergic neurons, immunohistochemical analysis was performed using an antibody against tryptophan hydroxylase-1 (TPH-1), an enzyme involved in the biosynthesis of serotonin. As previously reported, in situ analysis of brain sections using the synemin probe-3 demonstrated that the synemin transcript was expressed in neurons scattered within a square in Figure 3A. This region contains the midbrain and pons. As a means of quantitating the number of cells that express synemin, synemin transcript–positive neurons from the midbrain and pons were counted from seven different brain sections. The mean number of neurons was 33.1 (range 10–59). Obvious synemin staining was most apparent at high magnification (Fig. 3B). At even higher magnification (100×), large numbers of synemin-positive neurons were visible on the dorsal side of midbrain and pons (Fig. 3D). Detailed analysis of the square designated in Figure 3D showed synemin expression in large round neurons (Fig. 3F). Mirror sections were used to determine colocalization with immunostained proteins, because these sections provide greater resolution than serial sections when the positively labeled structures are small. In mirror sagittal sections, neurons demonstrated convincing colocalization of synemin transcript (Fig. 3B, D, and F) with TPH-1 protein (Fig. 3C, E, and G).

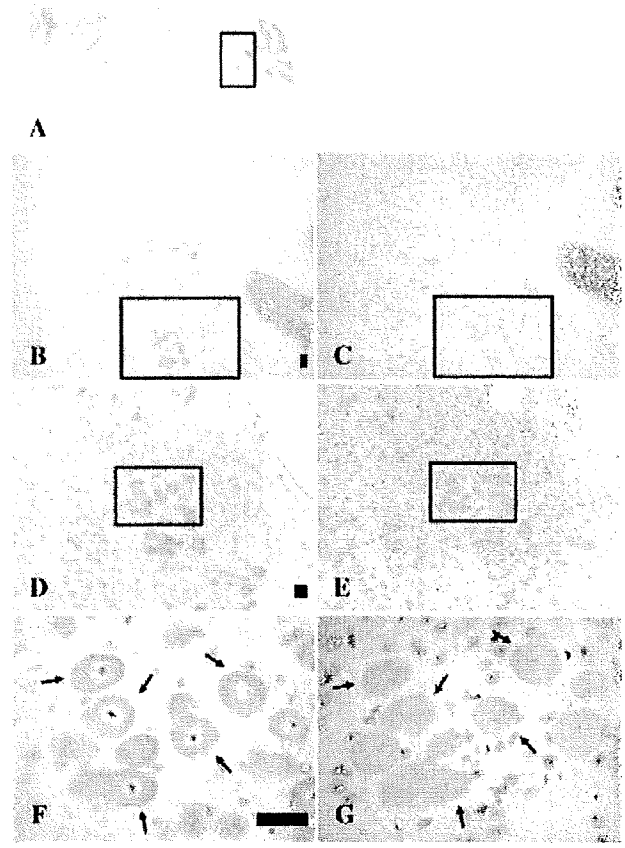

FIGURE 3. Colocalization of synemin transcript and tryptophan hydroxylase-1 protein (TPH-1) in brain sagittal sections. Panels **(A)**, **(B)**, **(D)**, and **(F)** are in situ experiments hybridized with the synemin probe-3, whereas panels **(C)**, **(E)**, and **(G)** are mirror sections of panels **(B)**, **(D)**, and **(F)** and are immunostained with an anti–tryptophan hydroxylase-1 antibody. Light purple designates in situ–positive structures, whereas orange indicates immunostaining with the anti–TPH-1 antibody. Panel **(A)** shows a whole sagittal brain where signals with probe-3 are seen inside the square. Panels **(B)**, **(D)**, and **(F)** are magnifications of panels **(A)**, **(B)**, and **(D)**, respectively. Squares in **(B)** and **(C)** show the same area as well as those in **(D)** and **(E)**. Arrows in **(F)** and **(G)** indicate the same neurons. Panels **(B)** and **(C)** are magnified 50×, **(D)** and **(E)** are 100×, and **(F)** and **(G)** are 400×. Bar = 50 μm.

DISCUSSION

Previous studies examined synemin expression in muscle[14] or whole brain.[13] In the brain, synemin transcript and protein are expressed in the large and round neurons of the midbrain and pons.[13] The purpose of the present study was to examine synemin expression in the spinal cord using in situ and immunohistochemical analyses to help hypothesize what its function might be in neuronal tissue. In contrast to a previous report,[8] which did not detect synemin protein in the anterior horn cells of the mouse spinal cord, Figures 1 and 2 show, by both in situ hybridization and immunohistochemical analyses, that synemin is weakly, but specifically expressed in those cells. It is possible that the difference between the two studies is due to the varying sensitivities of the two protocols used. For example, different

antibodies and tissue conditions were tested in these analyses.

Because synemin has been shown to interact in vitro with dystrophin[3] and α-dystrobrevin-1 (a known dystrophin-binding protein), its expression in the spinal cord of dystrophic mice (dystrophin null) was examined. The *mdx* mouse is a naturally isolated mutant that lacks dystrophin[24] and has been used to show that the expression of other muscle proteins is affected in the diseased state. For example, the sarcoglycans[19] are partially downregulated due to the loss of dystrophin and destabilization of the dystrophin-associated protein complex,[20] whereas utrophin, a dystrophin homolog, is more highly expressed and can partially compensate for the lack of dystrophin.[15] In addition to muscle, dystrophin isoforms are also expressed in other tissues, including brain. For example: (1) Dp260 is expressed in the retina, brain, and cardiac tissue[6]; (2) Dp140 is expressed throughout the central nervous system[10]; and (3) Dp71 is expressed more ubiquitously with the exception of skeletal muscle.[9] To determine whether synemin expression was altered in dystrophin-deficient neurological tissue, its expression was investigated in normal and *mdx* mouse spinal tissue, and no significant differences were noted. This could be because synemin does not interact with dystrophin in the spinal cord or because synemin is not as highly expressed in spinal cord compared with other tissues. Experiments to colocalize synemin with specific dystrophin isoforms, such as Dp71,[9] Dp140,[10] and Dp260,[6] were unsuccessful, namely because the unique sequences between these isoforms are in exon 1 and are too short to make isoform-specific probes necessary for in situ hybridization.

Previous studies have also shown that β-synemin can interact with α-dystrobrevin-1 (as opposed to α-dystrobrevin-2) in skeletal muscle.[12] As such, it is possible that α- and β-synemin could specifically interact with α-dystrobrevin-1 in neurons of the midbrain and pons. This was tested using in situ hybridization experiments with an α-dystrobrevin-1–specific probe (321 bp; position 2068–2388 of GenBank Accession No. NM_207650) corresponding to the last 106 amino acids and its stop codon.[4] Signals from this experiment were weak, suggesting that α-dystrobrevin-1 is not highly expressed in neurons of the midbrain and pons. Because synemin is expressed in those cells, it appears that synemin associates with some other protein(s) in nerve tissue.

Some of the best evidence available for synemin function has been derived from its expression pattern. In the midbrain and pons, synemin is highly expressed in a limited number of neurons that coexpress various neurotransmitters such as serotonin. Serotoninergic nerve fibers are derived from the midline raphe nucleus between the medulla oblongata and midbrain, whereas cholinergic neurons are abundant in the basal nucleus of Meynert, nucleus of the diagonal band, medial septal nucleus of basal forebrain, laterodorsal tegmental nucleus, and pedunculopontine tegmental nucleus of the midbrain and pons. Because cholinergic neuron-specific antibodies (i.e., antibodies against choline-*O*-acetyltransferase) were unavailable for use in paraffin-embedded sections, mouse sections were analyzed using an antibody against tryptophan hydroxylase-1 (TPH-1) to distinguish serotoninergic nerve fibers. TPH is a rate-limiting enzyme involved in the synthesis of serotonin.[5] This enzyme hydroxylates the 5-position of tryptophan to form 5-hydroxytryptophan, which is then converted to serotonin by an aromatic L-amino acid decarboxylase. In humans, as well as in other mammals, there are two isoforms of TPH. These isoforms (types 1 and 2) are encoded by two different, but homologous genes.[29] TPH-1 is phosphorylated by cAMP-dependent protein kinase A[11] and is present in peripheral tissues such as heart, lung, kidney, duodenum, and adrenal gland, but it is also expressed in the central nervous system (CNS).[33] On the other hand, TPH-2 is expressed exclusively in neurons of the CNS.[33] The finding that synemin and TPH-1 are expressed in the same neurons suggests that these cells are serotoninergic nerve fibers, although synemin appears to be more widely distributed than the area of raphe nuclei, suggesting it may be expressed in other cells as well.

It is unknown what role synemin may play in neurological diseases, but dysbindin is a coiled-coil–containing and α-dystrobrevin-binding protein.[2] Mutations in the dysbindin gene have been linked to schizophrenia.[18,25] The association between dysbindin and neurological disease is supported by results in schizophrenic patients that show: (1) dysbindin mRNA levels are reduced in the dorsolateral prefrontal cortex[30]; and (2) dysbindin protein levels are reduced in the hippocampus.[27] In schizophrenic patients, the dorsolateral prefrontal cortex has been consistently found to be dysfunctional.[31] In normal brain, dysbindin mRNA is expressed in temporal cortex, frontal cortex, substantia nigra, basal ganglia, and amygdala,[30] indicating a wide distribution of dysbindin expression. In contrast, synemin expression in the brain is restricted to the midbrain and pons.[13] In addition, the finding by Talbot et al. that dysbindin is present in intrinsic glutamatergic neurons in the hippocampus[27] also contrasts with syn-

emin expression, which associates with serotoninergic nerve fibers. These results suggest that, although both dysbindin and synemin proteins bind to α-dystrobrevin in muscle, the two proteins likely perform very diverse roles in the brain.

As its function and localization in the brain is not well understood, it is difficult to predict what effect mutations in synemin would have on brain function. Because β-synemin is thought to function as a structural protein in muscle, it is possible that synemin also serves a structural role in neurons of midbrain and pons. To search for potential pathological implications, it will be important to elucidate whether synemin is localized to either presynaptic or postsynaptic sites (or both). Immunoelectron-microscopic analysis and the identification of synemin-binding partners in the brain will provide useful information.

In conclusion, this report has shown that synemin transcript and its protein are expressed in anterior horn cells in the mouse spinal cord, although the signals were relatively weak. This suggests that expression was not as high as that seen in regions of the midbrain and pons. If synemin expression was proportionate to its importance, these results would suggest a more influential role for this protein in the midbrain and pons. To investigate the role of synemin in nerve tissue, we returned to brain to identify other colocalizing proteins as a means to better characterize synemin-expressing cells. Our results show that synemin and TPH-1 are coexpressed in the same neurons. We may thus begin to speculate as to synemin's function. Continued characterization of synemin-expressing cells will allow us to begin to understand synemin's function and to help ascertain whether mutations in this gene could contribute to human muscle or psychiatric diseases.[17]

This work was supported by a Grant-in-Aid for Scientific Research (C) (20591016) from the Japan Society for the Promotion of Science to Y.M. L.M.K. is an investigator at the Howard Hughes Medical Institute.

REFERENCES

1. Bellin RM, Huiatt TW, Critchley DR, Robson RM. Synemin may function to directly link muscle cell intermediate filaments to both myofibrillar Z-lines and costameres. J Biol Chem 2001;276:32330–32337.
2. Benson MA, Newey SE, Martin-Rendon E, Hawkes R, Blake DJ. Dysbindin, a novel coiled-coil-containing protein that interacts with the dystrobrevins in muscle and brain. J Biol Chem 2001;276:24232–24241.
3. Bhosle RC, Michele DE, Campbell KP, Li Z, Robson RM. Interactions of intermediate filament protein synemin with dystrophin and utrophin. Biochem Biophys Res Commun 2006;346:768–777.
4. Blake DJ, Nawrotzki R, Peters MF, Froehner SC, Davies KE. Isoform diversity of dystrobrevin, the murine 87-kDa postsynaptic protein. J Biol Chem 1996;271:7802–7810.
5. Cooper JR, Melcer I. The enzymic oxidation of tryptophan to 5-hydroxytryptophan in the biosynthesis of serotonin. J Pharmacol Exp Ther 1961;132:265–268.
6. D'Souza VN, Nguyen TM, Morris GE, Karges W, Pillers DA, Ray PN. A novel dystrophin isoform is required for normal retinal electrophysiology. Hum Mol Genet 1995;4:837–842.
7. Granger BL, Lazarides E. Synemin: a new high molecular weight protein associated with desmin and vimentin filaments in muscle. Cell 1980;22:727–738.
8. Izmiryan A, Cheraud Y, Khanamiryan L, Leterrier JF, Federici T, Peltekian E, et al. Different expression of synemin isoforms in glia and neurons during nervous system development. Glia 2006;54:204–213.
9. Lederfein D, Levy Z, Augier N, Mornet D, Morris G, Fuchs O, et al. A 71-kilodalton protein is a major product of the Duchenne muscular dystrophy gene in brain and other nonmuscle tissues. Proc Natl Acad Sci USA 1992;89:5346–5350.
10. Lidov HG, Selig S, Kunkel LM. Dp140: a novel 140 kDa CNS transcript from the dystrophin locus. Hum Mol Genet 1995; 4:329–335.
11. McKinney J, Knappskog PM, Haavik J. Different properties of the central and peripheral forms of human tryptophan hydroxylase. J Neurochem 2005;92:311–320.
12. Mizuno Y, Guyon JR, Ishii A, Hoshino S, Ohkoshi N, Tamaoka A, et al. Beta-synemin expression in cardiotoxin-injected rat skeletal muscle. BMC Musculoskel Disord 2007;8:40.
13. Mizuno Y, Guyon JR, Okamoto K, Kunkel LM. Synemin expression in brain. Muscle Nerve 2007;36:497–504.
14. Mizuno Y, Guyon JR, Watkins SC, Mizushima K, Sasaoka T, Imamura M, et al. Beta-synemin localizes to regions of high stress in human skeletal myofibers. Muscle Nerve 2004;30: 337–346.
15. Mizuno Y, Nonaka I, Hirai S, Ozawa E. Reciprocal expression of dystrophin and utrophin in muscles of Duchenne muscular dystrophy patients, female DMD-carriers and control subjects. J Neurol Sci 1993;119:43–52.
16. Mizuno Y, Thompson TG, Guyon JR, Lidov HG, Brosius M, Imamura M, et al. Desmuslin, an intermediate filament protein that interacts with alpha-dystrobrevin and desmin. Proc Natl Acad Sci USA 2001;98:6156–6161.
17. Mizuno Y, Puca AA, O'Brien KF, Beggs AH, Kunkel LM. Genomic organization and single-nucleotide polymorphism map of desmuslin, a novel intermediate filament protein on chromosome 15q26.3. BMC Genet 2001;2:8.
18. Owen MJ, Craddock N, O'Donovan MC. Schizophrenia: genes at last? Trends Genet 2005;21:518–525.
19. Ozawa E, Mizuno Y, Hagiwara Y, Sasaoka T, Yoshida M. Molecular and cell biology of the sarcoglycan complex. Muscle Nerve 2005;32:563–576.
20. Ozawa E, Yoshida M, Suzuki A, Mizuno Y, Hagiwara Y, Noguchi S. Dystrophin-associated proteins in muscular dystrophy. Hum Mol Genet 1995;4:1711–1716.
21. Sadoulet-Puccio HM, Feener CA, Schaid DJ, Thibodeau SN, Michels VV, Kunkel LM. The genomic organization of human dystrobrevin. Neurogenetics 1997;1:37–42.
22. Sadoulet-Puccio HM, Khurana TS, Cohen JB, Kunkel LM. Cloning and characterization of the human homologue of a dystrophin related phosphoprotein found at the Torpedo electric organ post-synaptic membrane. Hum Mol Genet 1996;5:489–496.
23. Sadoulet-Puccio HM, Rajala M, Kunkel LM. Dystrobrevin and dystrophin: an interaction through coiled-coil motifs. Proc Natl Acad Sci USA 1997;94:12413–12418.
24. Sicinski P, Geng Y, Ryder-Cook AS, Barnard EA, Darlison MG, Barnard PJ. The molecular basis of muscular dystrophy in the mdx mouse: a point mutation. Science 1989;244:1578–1580.
25. Straub RE, Jiang Y, MacLean CJ, Ma Y, Webb BT, Myakishev MV, et al. Genetic variation in the 6p22.3 gene DTNBP1, the human ortholog of the mouse dysbindin gene, is associated with schizophrenia. Am J Hum Genet 2002;71:337–348.

26. Sun N, Critchley DR, Paulin D, Li Z, Robson RM. Human alpha-synemin interacts directly with vinculin and metavinculin. Biochem J 2008;409:657–667.
27. Talbot K, Eidem WL, Tinsley CL, Benson MA, Thompson EW, Smith RJ, et al. Dysbindin-1 is reduced in intrinsic, glutamatergic terminals of the hippocampal formation in schizophrenia. J Clin Invest 2004;113:1353–1363.
28. Titeux M, Brocheriou V, Xue Z, Gao J, Pellissier JF, Guicheney P, et al. Human synemin gene generates splice variants encoding two distinct intermediate filament proteins. Eur J Biochem 2001;268:6435–6448.
29. Walther DJ, Bader M. A unique central tryptophan hydroxylase isoform. Biochem Pharmacol 2003;66:1673–1680.
30. Weickert CS, Straub RE, McClintock BW, Matsumoto M, Hashimoto R, Hyde TM, et al. Human dysbindin (DTNBP1) gene expression in normal brain and in schizophrenic prefrontal cortex and midbrain. Arch Gen Psychiatry 2004;61: 544–555.
31. Weinberger DR, Berman KF. Prefrontal function in schizophrenia: confounds and controversies. Philos Trans R Soc Lond B Biol Sci 1996;351:1495–1503.
32. Xue ZG, Cheraud Y, Brocheriou V, Izmiryan A, Titeux M, Paulin D, et al. The mouse synemin gene encodes three intermediate filament proteins generated by alternative exon usage and different open reading frames. Exp Cell Res 2004; 298:431–444.
33. Zill P, Büttner A, Eisenmenger W, Bondy B, Ackenheil M. Regional mRNA expression of a second tryptophan hydroxylase isoform in postmortem tissue samples of two human brains. Eur Neuropsychopharmacol 2004;14:282–284.

Journal of Clinical Neuroscience 16 (2009) 954-959

Contents lists available at ScienceDirect

Journal of Clinical Neuroscience

journal homepage: www.elsevier.com/locate/jocn

Laboratory Study

Association of autophagy with cholesterol-accumulated compartments in Niemann-Pick disease type C cells

Seiya Ishibashi, Tsuneo Yamazaki *, Koichi Okamoto

Department of Neurology, Gunma University Graduate School of Medicine, 3-39-15 Showa-machi, Maebashi, Gunma 371-8511, Japan

ARTICLE INFO

Article history:
Received 12 August 2008
Accepted 16 September 2008

Keywords:
Autophagy
Cholesterol
Niemann-Pick disease type C
LC3

ABSTRACT

Niemann-Pick disease type C (NPC) is an autosomal recessive disease most commonly caused by a mutation of *NPC1*, resulting in the accumulation of cholesterol in late endosomes or lysosomes. In this study, we examined whether an abnormality of autophagy is involved in the pathogenesis of NPC and how cholesterol accumulation participates in this process, using both a U18666A-induced NPC model and NPC1-deficient Chinese hamster ovary cells. In these cells, an increase in the level of the microtubule-associated protein 1 light chain 3 (LC3-II) was demonstrated by Western blotting. An increase in the number of granular LC3-positive structures that colocalized with filipin-labeled accumulated cholesterol was also observed in morphological studies. Cholesterol depletion inhibited the formation of granular LC3-positive structures that colocalized with filipin-labeled cholesterol, and instead promoted the formation of ring-shaped LC3-positive filipin-negative structures in U18666A-treated cells. These results demonstrate the close association of the accumulation of LC3 with accumulated cholesterol in NPC cells.

1. Introduction

Niemann-Pick disease type C (NPC) is an autosomal recessive neurovisceral lipid storage disorder, clinically characterized by hepatosplenomegaly and neurodegeneration, resulting in progressive dementia, dystonia, ataxia and death, often in childhood.[1] Most cases of NPC are caused by a mutation in *NPC1*, resulting in the accumulation of free cholesterol in late endosomes or lysosomes. The *NPC1* gene encodes a multitransmembrane glycoprotein known as Niemann-Pick C1 protein (NPC1). NPC1 localizes to organelles that are positive for lysosome-associated membrane protein, presumably late endosomes and lysosomes.[2] Based on the cellular phenotype of NPC, NPC1 is important for the movement of free cholesterol and other cargo out of the late endosomes or lysosomes,[3] but the precise mechanisms of NPC pathogenesis remains unknown.

Autophagy is a system of bulk protein degradation and recycling, which is induced under starvation conditions.[4,5] When autophagy is induced, a portion of the cytoplasm and organelles are sequestered within a double-membrane-limited vacuole, the autophagosome.[6] A cytosolic form of microtubule-associated protein 1 light chain 3 (LC3), LC3-I, is rapidly conjugated with phosphatidylethanolamine to generate a membrane-bound form, LC3-II, and tightly incorporated into the autophagosomal membrane. Then, autophagosomes undergo a stepwise maturation, through acquisition of lysosomal membrane proteins, acidic pH, and proteolytic enzymes by fusing with early[7] and late endosomes as well as lysosomes,[8] to single-membrane autolysosomes, in which internal substrates are degraded and recycled back to the cytoplasm. LC3-II is also degraded or recycled back to cytosolic LC3-I. Thus, the amount of LC3-II correlates with the extent of autophagosomal formation,[9] and monitoring the level of LC3-II by Western blotting has been widely used for evaluating autophagic activity. Autophagosomes are also identified morphologically as small vesicular or large ring-shaped structures by labeling LC3-II incorporated into the membrane.[10]

Recently, an increase in the number of autophagosomes in various neurodegenerative diseases has been reported. However, in many cases it is unclear whether this is due to an increase in autophagic activity or inhibited removal of autophagosomes caused by impairment of maturation.[11] The same question arises in NPC pathology. The purpose of this study is to examine whether an abnormality of autophagy is involved in the pathogenesis of NPC and how cholesterol participates in this process, using a drug-induced NPC model and NPC1-deficient cultured Chinese hamster ovary (CHO) cells. Our findings demonstrate that an increase in the level of LC3-II in NPC cells does not reflect an increase in autophagic activity but an accumulation of LC3-II, in close association with an accumulation of cholesterol.

2. Materials and methods

2.1. Antibodies

A rabbit anti-LC3 antibody used for Western blotting was kindly provided by Dr T. Yoshimori (Research Institute for Microbial

* Corresponding author. Tel.: +81 272 20 8064; fax: +81 272 20 8068.
E-mail address: tsuneoy@med.gunma-u.ac.jp (T. Yamazaki).

0967-5868/$ - see front matter © 2008 Elsevier Ltd. All rights reserved.
doi:10.1016/j.jocn.2008.09.020

Diseases, Osaka University, Japan).[9] A rabbit anti-LC3 antibody used for immunofluorescence labeling (Santa Cruz Biotechnology, Santa Cruz, CA, USA), a goat anti-rabbit IgG HRP-conjugated secondary antibody and an anti-rabbit IgG antibody conjugated to Alexa Fluor 488 (Invitrogen, Carlsbad, CA, USA) were purchased.

2.2. Cells and cell culture

Wild-type CHO cells were kindly provided by Dr E.H. Koo (Department of Neuroscience, University of California San Diego).[12] CHO-JP17 (a cell line expressing a retrovirus receptor and used as a control for NPC1-deficient CHO) and NPC1-deficient CHO (the NPC1 locus of CHO-JP17 was disrupted by retrovirus-mediated gene trap mutagenesis) cells[13] were kindly provided by Dr H. Ninomiya (Tottori University Faculty of Medicine, Yonago, Japan). For amino acid (AA) starvation, cells were incubated in Hanks' balanced salt solution (HBSS) for 1 hour. For generating NPC model cells mimicking the features of the NPC phenotype, cells were incubated with 3 μg/mL of class 2 amphiphile U18666A (Biomol, Plymouth Meeting, PA, USA) for 24 hours. For cholesterol depletion, cells

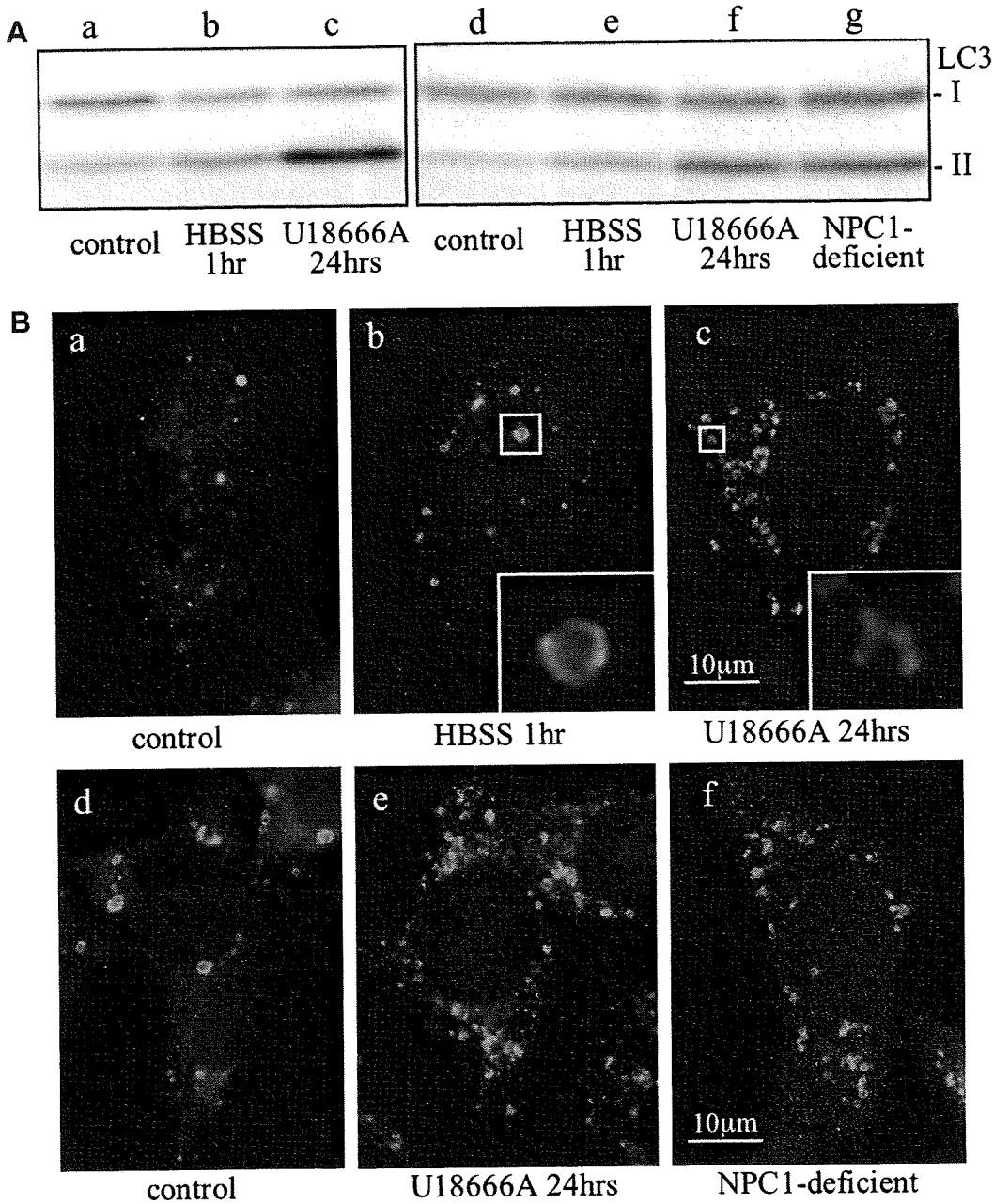

Fig. 1. (A) Western blotting using anti-LC3 antibody. (a–c) Lysates from wild-type Chinese hamster ovary (CHO) cells incubated in full nutrient medium (control) and Hanks' balanced salt solution (HBSS) for 1 hour and treated with U18666A for 24 hours showing an increase in the level of the microtubule-associated protein 1 light chain 3 (LC3)-II, indicating autophagic activity in Niemann-Pick disease type C (NPC) model cells. (d–g) Lysates from CHO-JP17 cells incubated in full nutrient medium (control) and HBSS for 1 hour and treated with U18666A for 24 hours, and NPC1-deficient cells showing an increase in the level of LC3-II in NPC model and NPC1-deficient cells. (B) Immunofluorescence labeling using anti-LC3 antibody. (a–c) Wild-type CHO cells incubated in full nutrient medium (control) and HBSS for 1 hour and treated with U18666A for 24 hours showing an increase in the number of granular LC3-positive structures in NPC model cells. (d–f) CHO-JP17 cells, incubated in full nutrient medium (control) and treated with U18666A for 24 hours, and NPC1-deficient cells showing an increase in the number of granular LC3-positive structures in the NPC model and NPC1-deficient cells. Bar, 10 μm. Lower right panels are enlarged images of the corresponding rectangular areas. Results are representative of triplicate experiments with similar results.

were incubated in Dulbecco's modified essential medium (DMEM) with 10% lipoprotein-deficient fetal calf serum (LPDS) in the presence of 20 μM mevastatin and 230 μM mevalonolactone (Sigma-Aldrich, St Louis, MO, USA).

2.3. Western blotting

Cell lysates containing equal amounts of protein (10–20 μg per lane) were electrophorezed in 15% acrylamide gels and transferred to polyvinylidene difluoride (PVDF) membranes. Immunoblot analysis was performed using indicated antibodies and the signals of immunoreactivity were detected using an enhanced chemiluminescence (ECL) Western blotting detection system (Amersham Biosciences, Piscatway, NJ, USA).

2.4. Immunofluorescence labeling

Cells grown on glass coverslips were fixed in 4% paraformaldehyde and 4% sucrose. After permeabilization with 1% Triton X-100 and blocking with 10% fetal bovine serum (FBS) in phosphate buffered saline (PBS), cells were reacted with the anti-LC3 antibody at a dilution of 1:50 for 1 hour, followed by incubation with the Alexa-labeled secondary antibody. For visualizing free cholesterol, cells were incubated with 0.05 mg/mL filipin (Sigma-Aldrich, St Louis, MO, USA) for 1 hour. Filipin is a fluorescent antibiotic with a high affinity for cholesterol and is therefore frequently used for specifically labeling free cholesterol.[14] Images were then captured under an Olympus BX50 microscope and examined using the attached software (Olympus, Tokyo, Japan).

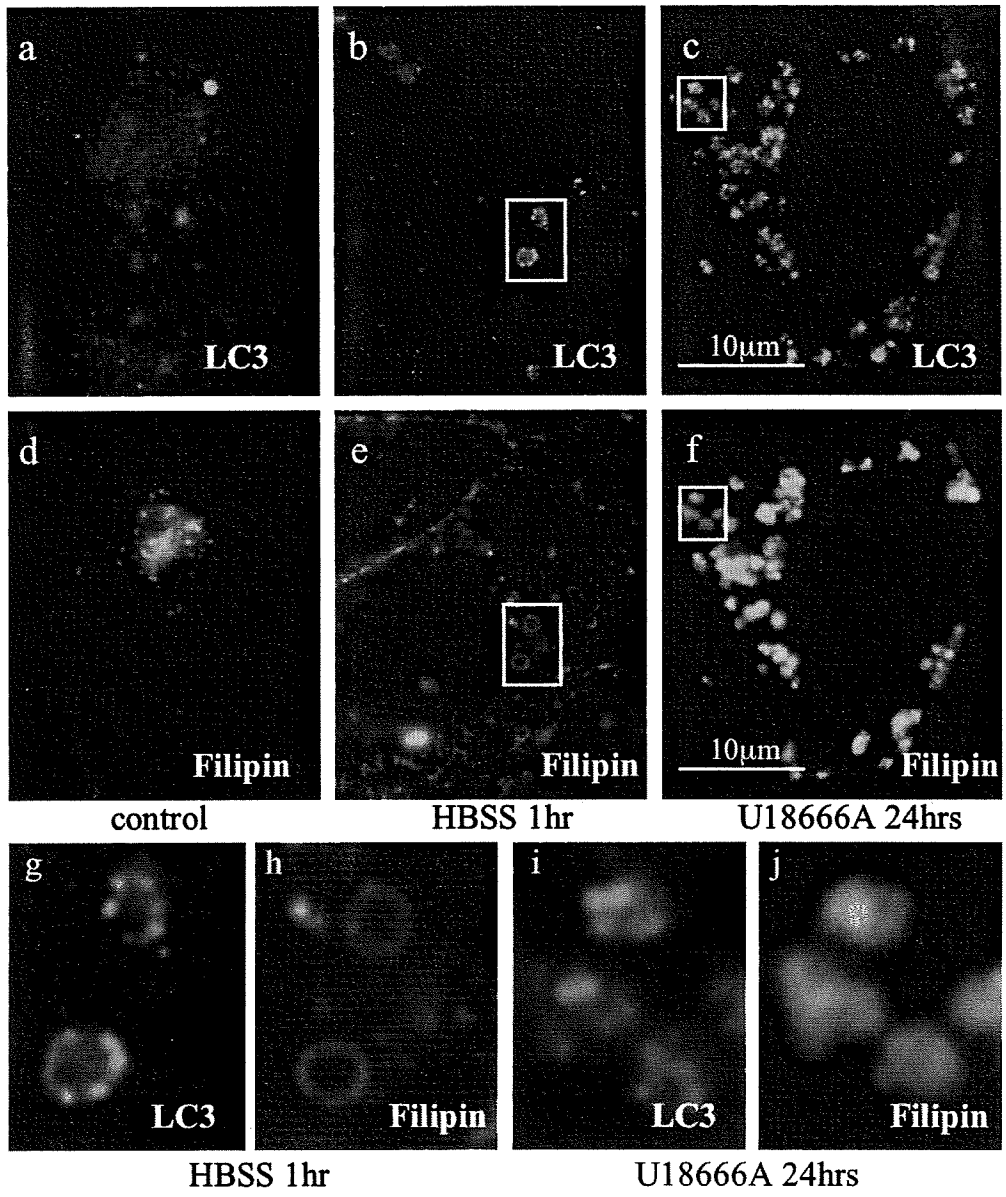

Fig. 2. Immunofluorescence labeling using anti-LC3 antibody (a–c) and double staining with filipin (d–f). (a–f) Wild-type Chinese hamster ovary (CHO) cells incubated in full nutrient medium (control) and Hanks' balanced salt solution (HBSS) for 1 hour, and treated with U18666A for 24 hours. Enlarged images of corresponding rectangular areas of wild-type CHO cells incubated in HBSS for 1 hour (g, h) showing ring-shaped LC3-positive structures completely rimmed by filipin in amino acid-starved cells, and treated with U18666A for 24 hours (i, j) showing colocalization of granular LC3-positive structures with filipin-labeled accumulated cholesterol in NPC model cells. Bar, 10 μm. Results are representative of triplicate experiments with similar results.

3. Results

3.1. The level of LC3-II and number of LC3 positive structures increased in NPC cells

To evaluate autophagic activity in NPC cells, we first examined U18666A-treated NPC model cells. In wild-type CHO (Fig. 1Ac) and CHO-JP17 (Fig. 1Af) cells treated with U18666A, the level of LC3-II determined by Western blotting was markedly higher than those in AA-starved cells (Figs. 1Ab,e). The same result was obtained in NPC1-deficient cells (Fig. 1Ag). Next, we examined the morphological changes of autophagosomes by immunofluorescence labeling of LC3. In wild-type CHO cells, distinctly ring-shaped LC3-positive structures, which were rarely observed in control cells (Fig. 1Ba), increased in number, and accumulated around the nucleus following AA starvation (Fig. 1Bb). Following U18666A treatment, LC3-positive structures markedly increased in number, and distributed diffusely in the cell (Fig. 1Bc). Similar results were obtained in U18666A-treated CHO-JP17 (Fig. 1Be) and NPC1-deficient cells (Fig. 1Bf). Thus, the level of LC3-II determined by Western blotting and the number of LC3-positive structures determined by immunofluorescence labeling increased in NPC cells.

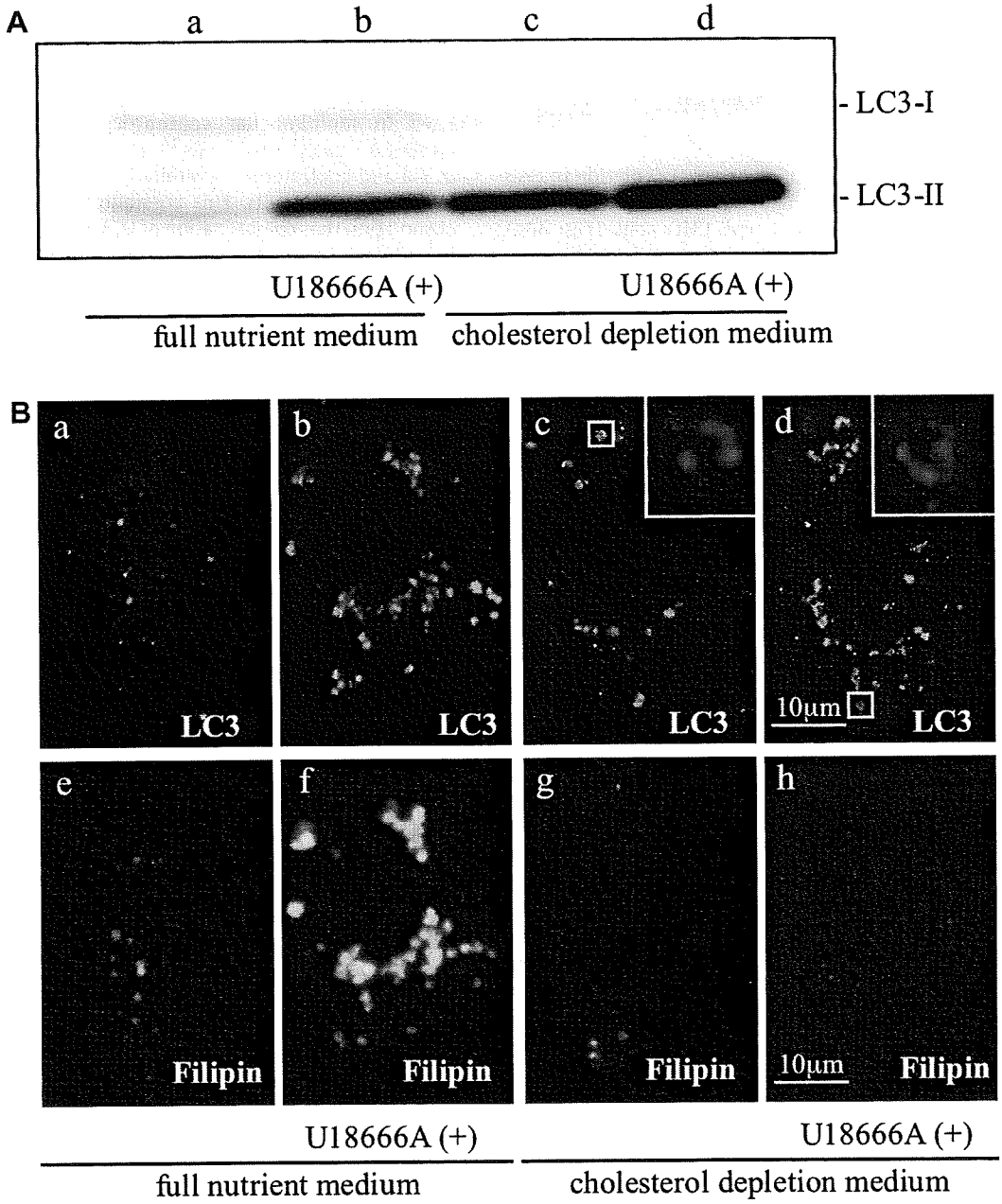

Fig. 3. Effects of cholesterol depletion in wild-type Chinese hamster ovary (CHO) cells treated with U18666A. Wild-type CHO cells were cultured in full nutrient medium (Dulbecco's modified essential medium, DMEM, with 10% fetal bovine serum), or cholesterol depletion medium (DMEM with 10% lipoprotein-deficient fetal calf serum, 20 μM mevastatin and 230 μM mevalonolactone) for 2 days, with or without U18666A for the last 24 hours. (A) Western blotting using anti-microtubule-associated protein 1 light chain 3 (LC3) antibody showing an additional effect of cholesterol depletion on increasing the level of LC3-II in U18666A-treated cells. (B) Immunofluorescence labeling using anti-LC3 antibody and double staining with filipin showing that cholesterol depletion inhibited the formation of granular LC3-positive structures that colocalized with filipin-labeled cholesterol, and instead promoted the formation of ring-shaped LC3-positive filipin-negative structures in U18666A-treated cells. Bar, 10 μm. Upper right panels are enlarged images of corresponding rectangular areas. Results are representative of triplicate experiments with similar results.

3.2. LC3 and cholesterol are accumulated in the same structures in U18666A-treated cells

Next, we compared the distribution of LC3 labeling with that of filipin. In control wild-type CHO cells, LC3-positive structures were rarely stained by filipin (Figs. 2a,d). In AA-starved cells, ring-shaped LC3-positive structures (Figs. 2b,g) were sometimes completely rimmed by filipin (Figs. 2e,h). In U18666A-treated cells, accumulated cholesterol was stained by filipin and was observed as coarse round structures (Fig. 2f), and a large part of, but not all of, these structures were also positive for LC3 (Fig. 2c). In a detailed observation, these structures were almost uniformly stained by filipin (Fig. 2j), but LC3 labeling was granular in shape, with an irregular appearance (Fig. 2i). On the basis of these observations, it was inferred that LC3 is accumulated in the same structures as those where cholesterol is accumulated in NPC cells.

3.3. Form of LC3 labeling in U18666A-treated cells is changed by cholesterol depletion

Finally, we examined the effect of cholesterol depletion in cells treated with U18666A. In Western blotting, the level of LC3-II increased in cholesterol-depleted wild-type CHO cells (Fig. 3Ac), and U18666A treatment in addition to cholesterol depletion induced a more prominent increase in LC3-II level (Fig. 3Ad). However, immunofluorescence labeling showed that the number of LC3-positive filipin-labeled structures following U18666A treatment (Figs. 3Bb,f) markedly decreased in cholesterol-depleted cells (Fig. 3Bd). Instead, the number of ring-shaped LC3-positive structures increased, and LC3 labeling did not correspond with filipin staining (Figs. 3Bd,h). Thus, cholesterol depletion in U18666A-treated cells had an additional effect of increasing the level of LC3-II, as determined by Western blotting, but inhibited the accumulation of LC3 within structures where cholesterol is accumulated, and instead promoted the formation of ring-shaped LC3-positive structures.

4. Discussion

Cheng et al. demonstrated that an acute decrease in the level of cell membrane cholesterol induced by methyl-β-cyclodextrin or nystatin treatment increased the level of LC3-II, as determined by Western blotting, and increases the number of LC3-positive structures, as determined by morphological observation.[15] They also showed that cholesterol depletion induced by treatment with LPDS and mevastatin/mevalonolactone for 2 to 3 days caused an increase in the level of LC3-II, as determined by Western blotting, and an increase in the number of LC3-positive structures, as determined by immunofluorescence labeling. They suggested that these are caused by the retardation of autophagosome maturation.

The question is how cholesterol participates in autophagic maturation. Eskelinen et al. showed that nascent autophagosomes have no detectable cholesterol, but during their maturation from early to late autophagosomes, the cholesterol content in the limiting membrane gradually increases.[16] In our study, ring-shaped LC3-positive structures formed by cholesterol depletion were not stained by filipin, and are thus supposed to be nascent or immature autophagosomes. The exact role of cholesterol in late autophagosomes remains unclear, but it is possible that the higher cholesterol content in late autophagosomes is required to protect the limiting membranes of the vacuoles against proteolytic enzymes.[17] Therefore, cholesterol depletion may interrupt autophagosome maturation, resulting in the accumulation of immature autophagosomes and an increase in the level of LC3-II.

The issue we have to consider next is whether an increase in the level of LC3-II in NPC cells is caused by the mechanism similar to that induced by cholesterol depletion. From our results, cholesterol depletion in U18666A-treated cells had an additional effect of increasing the level of LC3-II, as demonstrated by Western blotting, and the shape of LC3-positive structures formed following U18666A treatment was different from that formed following cholesterol depletion. Thus, the causal mechanisms underlying the increase in the level of LC3-II induced by U18666A treatment and cholesterol depletion were apparently different. Moreover, LC3-positive structures formed following U18666A treatment colocalized with filipin staining. These results indicated that an increased level of LC3-II following U18666A treatment reflect the abnormal accumulation of LC3-II within the structure where cholesterol is accumulated.

In view of the fact that LC3-II is a membranous component of autophagosomes, it is noteworthy that LC3-positive structures in NPC cells were not ring-shaped but granular-shaped, as demonstrated in our morphological study. Cholesterol is also transported as a membranous component in cells, and therefore it is accumulated in multilamellar concentric lipid membrane layers in U18666A-treated CHO cells.[18] These observations indicate that LC3-II and cholesterol are similarly accumulated in the endocytic pathway of NPC cells. This possibility may be supported by our observation that colocalization of LC3 and accumulated cholesterol in U18666A-treated cells was inhibited with cholesterol depletion. However, further morphological examinations are required to elucidate the precise mechanisms.

In conclusion, this study showed that an increase in the level of LC3-II is caused by accumulation of LC3 in close association with cholesterol accumulation in NPC cells, and cholesterol plays an important role in autophagy. Further research on the precise mechanisms of autophagic maturation associated with cholesterol may provide new insights into the mechanisms underlying the pathogenesis of NPC.

Acknowledgments

This work was supported by grants from the Ministry of Health, Labour and Welfare of Japan, and also from the Ministry of Education, Culture, Sports, Science and Technology of Japan to K. Okamoto (No. 18590926).

References

1. Vanier MT, Millat G. Niemann-Pick disease type C. *Clin Genet* 2003 [illegible]
2. Scott C, Ioannou YA. The NPC1 protein: structure implies functi[illegible] *Biophys Acta* 2004;**1685**:8–13.
3. Neufeld EB, Wastney M, Patel S, et al. The Niemann-Pick C1 protein resides in a vesicular compartment linked to retrograde transport of multiple lysosomal cargo. *J Biol Chem* 1999;**274**:9627–35.
4. Klionsky DJ, Emr SD. Autophagy as a regulated pathway of cellular degradation. *Science* 2000;**290**:1717–21.
5. Yoshimori T. Autophagy: a regulated bulk degradation process inside cells. *Biochem Biophys Res Commun* 2004;**313**:453–8.
6. Dunn Jr WA. Studies on the mechanisms of autophagy: formation of the autophagic vacuole. *J Cell Biol* 1990;**110**:1923–33.
7. Liou W, Geuze HJ, Geelen MJ, et al. The autophagic and endocytic pathways converge at the nascent autophagic vacuoles. *J Cell Biol* 1997;**136**: 61–70.
8. Dunn Jr WA. Autophagy and related mechanisms of lysosome-mediated protein degradation. *Trends Cell Biol* 1994;**4**:139–43.
9. Kabeya Y, Mizushima N, Ueno T, et al. LC3, a mammalian homologue of yeast Apg8p, is localized in autophagosome membranes after processing. *EMBO J* 2000;**19**:5720–8.
10. Jäger S, Bucci C, Tanida I, et al. Role for Rab7 in maturation of late autophagic vacuoles. *J Cell Sci* 2004;**117**:4837–48.
11. Rubinsztein DC, DiFiglia M, Heintz N, et al. Autophagy and its possible roles in nervous system diseases, damage and repair. *Autophagy* 2005;**1**:11–22.
12. Koo EH, Squazzo SL. Evidence that production and release of amyloid beta-protein involves the endocytic pathway. *J Biol Chem* 1994;**269**:17386–9.
13. Higaki K, Ninomiya H, Sugimoto Y, et al. Isolation of NPC1-deficient Chinese hamster ovary cell mutants by gene trap mutagenesis. *J Biochem* 2001;**129**:875–80.

14. Börnig H, Geyer G. Staining of cholesterol with the fluorescent antibiotic "filipin". *Acta Histochem* 1974;**50**:110–5.
15. Cheng J, Ohsaki Y, Tauchi-Sato K, et al. Cholesterol depletion induces autophagy. *Biochem Biophys Res Commun* 2006;**351**:246–52.
16. Eskelinen EL. Maturation of autophagic vacuoles in Mammalian cells. *Autophagy* 2005;**1**:1–10.
17. Punnonen EL, Pihakaski K, Mattila K, et al. Intramembrane particles and filipin labeling on the membranes of autophagic vacuoles and lysosomes in mouse liver. *Cell Tissue Res* 1989;**258**:269–76.
18. Lusa S, Blom TS, Eskelinen EL, et al. Depletion of rafts in late endocytic membranes is controlled by NPC1-dependent recycling of cholesterol to the plasma membrane. *J Cell Sci* 2001;**114**:1893–900.

NEUROPATHOLOGY

Neuropathology 2009; **29**, 566–573 doi:10.1111/j.1440-1789.2009.01017.x

Original Article

Regional distribution of TDP-43 inclusions in Alzheimer disease (AD) brains: Their relation to AD common pathology

Ai Kadokura,[1] Tsuneo Yamazaki,[1] Cynthia A. Lemere,[2] Masamitsu Takatama[3] and Koichi Okamoto[1]

[1]Department of Neurology, Gunma University Graduate School of Medicine, Gunma, Japan, [2]Center for Neurologic Diseases, Brigham and Women's Hospital, Harvard Medical School, USA, and [3]Geriatric Research Institute and Hospital, Gunma, Japan

Initially, trans activation responsive region (TAR)-DNA-binding protein 43 (TDP-43) was considered to be a disease-specific component of ubiquitin-positive and tau-negative inclusions in the brains of patients with frontotemporal lobar degeneration with ubiquitin-positive inclusions (FTLD-U) and amyotrophic lateral sclerosis (ALS); however, it is now widely known that this protein also abnormally accumulates in neurons in other neurodegenerative diseases. On the basis of observation mainly in the medial temporal lobe, TDP-43-immunoreactive neuronal inclusions have been detected in 20–30% of Alzheimer disease (AD) brains. However, it is controversial whether these cases represent a combined disease, that is, mixed AD/FTLD-U. To address this issue, it is necessary to obtain more knowledge on the region-specific distribution of TDP-43 immunoreactivity and also about its relationship to AD common pathology. Here, we describe abnormal TDP-43 immunoreactivity in the medial temporal lobe in 5/16 AD patients (31%). Most of the depositions were cytoplasmic inclusions, mainly located in the subiculum and parahippocampal gyrus and rarely in dentate granular cells of the hippocampus. TDP-43-positive inclusions and senile plaque/neurofibrillary tangle distribution were not always identical, and intracellular colocalizations of TDP-43 and phospho-tau were also infrequent. The cases showing TDP-43-positive inclusions in the medial temporal lobe also showed abnormally highly dense TDP-43 immunoreactivity in the frontal, but not in the parietal and occipital cortices. Intracellularly, TDP-43-positive inclusions were highly ubiquitinated and colocalized with p62 immunoreactivity as well. Our findings suggest that abnormal TDP-43 deposition and AD pathology (formation of senile plaques and neurofibrillary tangles) might occur independently. However, taken together with the results of previous reports, the distribution of TDP-43 immunoreactivity in the hippocampus and frontal cortex in AD appear to be varying. We consider that it is still too early to determine that the TDP-43 accumulation is a part of AD pathology or result from a completely independent pathology.

Key words: Alzheimer disease, p62, tau, TDP-43, ubiquitin.

INTRODUCTION

The TAR-DNA-binding protein 43 (TDP-43) has recently been identified as a major disease protein in the ubiquitinated inclusions in frontotemporal lobar degeneration (FTLD) with ubiquitin-positive and tau-negative inclusions (FTLD-U) and amyotrophic lateral sclerosis (ALS).[1] This is consistent with the hypothesis that these diseases represent a clinicopathological spectrum of disorders that can be subsumed under the term TDP-43 proteinopathies.[2,3] The initial findings of TDP-43 as the most specific marker for the detection of neuronal inclusions and neurites in FTLD-U and ALS have been rapidly confirmed by others.[4–9] However, subsequent studies have indicated that TDP-43-positive inclusions can be detected in other neurodegenerative disorders, including Parkinson disease dementia and dementia with Lewy bodies,[10] parkinsonism–dementia complex and ALS in Guam,[11,12] and in corticobasal degeneration.[13]

In Alzheimer disease (AD), Amador-Ortiz *et al.* first described abnormal TDP-43 accumulation in the

Correspondence: Tsuneo Yamazaki, MD, PhD, Department of Neurology, Gunma University Graduate School of Medicine, 3-39-22 Showamachi, Maebashi, Gunma 371-8511, Japan. Email: tsuneoy@med.gunma-u.ac.jp

Received 20 October 2008; revised and accepted 6 February 2009; published online 26 April 2009.

hippocampal region in as many as 20% of cases,[14] and this result was followed by other groups.[13,15,16] Now, it has become a consensus that approximately 20–34% of AD patients' brains contain TDP-43-positive neuronal inclusions. However, these results were derived from studies examining mainly hippocampal regions, and whether the presence of TDP-43 -positive inclusions in AD subjects represents concomitant AD and FTLD-U or an independent phenomenon is controversial.[14-16] To address this issue, it is essential to obtain more knowledge on the region-specific distribution of TDP-43-positive inclusions in AD and also on its immunological localization with the AD common pathology. In this study, we attempted to examine TDP-43 immunoreactivity in a new series of AD specimens and describe the detailed distribution of TDP-43-positive neuronal inclusions in comparison with the AD pathology.

MATERIALS AND METHODS

Sixteen AD subjects (average age: 74.8 years; 6 males, 10 females) that showed clinically probable AD (Consortium to Establish a Registry for Alzheimer's Disease [CERAD] C)[17] and AD-type pathologic changes that met the criteria for at least intermediate-probability AD[18] were selected.

Five-micrometer-thick sections of formalin-fixed, paraffin-embedded tissue from the medial temporal lobe containing hippocampus, entorhinal cortex, and occipitotemporal gyrus were immunostained with antibodies against TDP-43 (10782-1-AP: rabbit polyclonal antibody; Protein Tech Group, Chicago, IL, US) using the streptoavidin-biotin method (Histofine SAB-PO kit; Nichirei, Tokyo, Japan). In a subset of cases, immunostaining was also performed with a mouse monoclonal anti-TDP-43 antibody (Abnova Corporation, Taipei, Taiwan). Serial sections were stained with antibodies against amyloid β (6E10: Covance Research Products, Emeryville, CA, US), phospho-tau (AT8: Innogenetics, Ghent, Belgium), and α-synuclein.[19] Immunoreactivity was visualized with 0.5 mg/mL 3,3,-diaminobenzidine tetrachloride (DAB) and 0.03% hydrogen peroxide (Dojin Laboratories, Kumamoto, Japan) or VIP (Vector, Burlingame, CA, US). All the sections were counterstained with hematoxylin. For retrieving antigens in TDP-43 and 6E10 staining, the sections were autoclaved for 5 min or treated with 70% formic acid for 10 min, respectively. The specimens were observed under an Olympus BX60 (Olympus, Tokyo, Japan) using the DP Controller system (Olympus). In all the cases with TDP-43-positive inclusions in these sections, additional immunohistochemistry was performed on sections from the frontal, parietal and occipital cortex.

To examine the detailed TDP-43 localization, the sections were double-labeled with the rabbit polyclonal anti-TDP-43 and mouse monoclonal anti-AT8, anti-ubiquitin (Chemicon, Temecula, CA, US) or guinea pig polyclonal anti-p62 (GP62N; Progen, Heidelberg, Germany) antibodies. After washing with phosphate-buffered saline, the sections were subsequently treated in a cocktail of secondary antibodies: goat anti-rabbit Alexa Fluor 488 and goat anti-mouse Alexa Fluor 568 or goat anti-guinea pig Fluor 568 (Molecular Probes-Invitrogen, Eugene, OR, US). To avoid autofluorescence signaling, the sections were pretreated with Sudan Black B for 5 min and rinsed in 70% ethanol. The specimens were examined under a microscope with fluorescent (BX50: Olympus, Tokyo, Japan) or confocal (FV1000: Olympus) systems. The obtained images were further processed using Adobe Photoshop CS2 ver.9 (Adobe, San Jose, CA, US).

RESULTS

We first examined the distribution of TDP-43 deposition in the medial temporal cortex of AD cases. TDP-43-positive inclusions were found in 5/16 AD cases (31%) and were predominantly observed in the subiculum and parahippocampal gyrus (Fig. 1a–d). In these cases, TDP-43-positive inclusions were distributed in the middle and upper cortical layers and rarely observed in neurons of the dentate granule cell layer of the hippocampus (Fig. 1e). In 4/5 cases, TDP-43 immunoreactivity extended over the collateral sulcus into the occipitotemporal gyrus (Fig. 2a,c), while the topographical distribution ended at the bottom of the sulcus in one case (Fig. 2b,d). Most TDP-43-positive inclusions predominantly appeared as neuronal cytoplasmic inclusions (Fig. 1b,d); thus, our cases were partially close to type 3 of the classification scheme for ubiquitin-positive inclusions of FTLD-U by Mackenzie *et al.*[20] and type 2 by Cairns *et al.*[21]

Next, we attempted to compare the distribution of TDP-43-positive inclusions with AD pathologies, namely, senile plaques and neurofibrillary tangles in the TDP-43 positive cases. For this purpose, serial AD sections were immunolabeled with anti-TDP-43 and anti-amyloid β or anti-phospho-tau antibodies. TDP-43, amyloid β, and phospho-tau immunoreactivities were detected in the hippocampal and parahippocampal regions. However, in one case, senile plaques and neurofibrillary tangles were independently located in the occipitotemporal gyrus apart from the TDP-43 deposition (Fig. 3a–c). We also compared the TDP-43 distribution with those of α-synuclein in the medial temporal lobe; however, almost no α-synuclein immunoreactivity was detected in our subjects (data not shown).

To observe the detailed specificity of TDP-43-positive neuronal inclusions, AD sections were double-labeled with TDP-43 and AT8. Whereas AT8 strongly labeled numbers of neurofibrillary tangles and neuropil threads, TDP-43

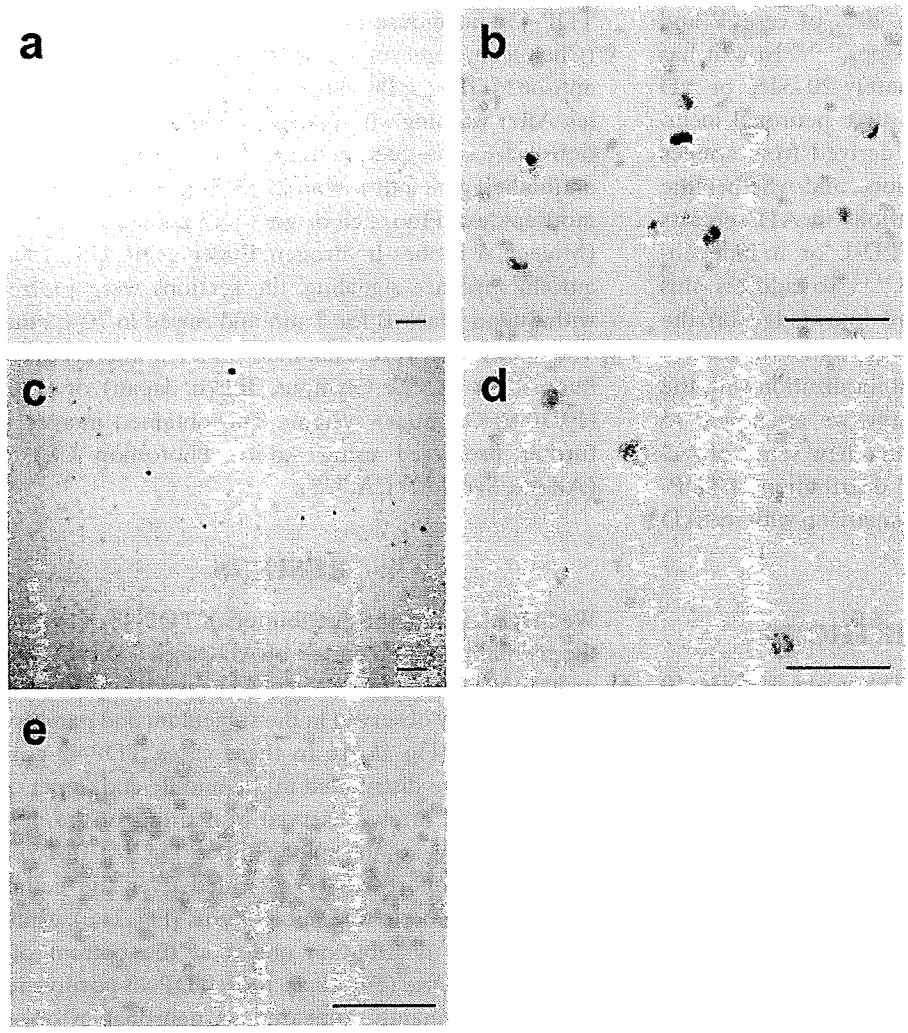

Fig. 1 Immunohistochemical feature of TAR-DNA-binding protein 43 (TDP-43) pathology in medial temporal lobe of Alzheimer disease (AD) patients. Abnormal TDP-43 immunoreactivity is predominantly observed in the middle and upper cortical layers of the parahippocampal gyrus (a, b) and subiculum (c, d). Practically all the TDP-43 is accumulated as intracytoplasmic neuronal inclusions (b, d). Although the abnormal TDP-43 deposition in the neurons of the dentate granule cell layer of the hippocampus is crucial in frontotemporal lobar degeneration with ubiquitin-positive and tau-negative inclusions (FTLD-U), it is difficult to find the accumulation of the protein in this area in our AD cases (e). Scale bars: a and c, 100 μm; b, d and e, 50 μm.

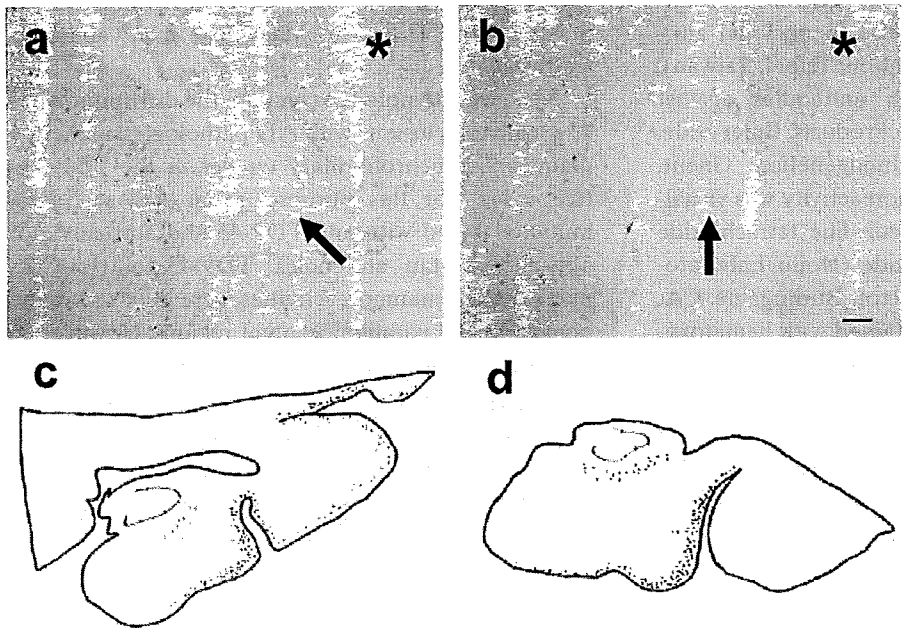

Fig. 2 In 4/5 cases, the TAR-DNA-binding protein 43 (TDP-43) immunoreactivity in the parahippocampal gyrus extends over the collateral sulcus (arrow) into the occipitotemporal gyrus (*) (a, c), while the immunoreactivity is restricted in the hippocampus, subiculum, and parahippocampal gyrus in one case (b, d). (c) and (d) are topographical distributions of TDP-43 inclusions in the medial temporal lobes of two representative cases. Scale bar: 100 μm.

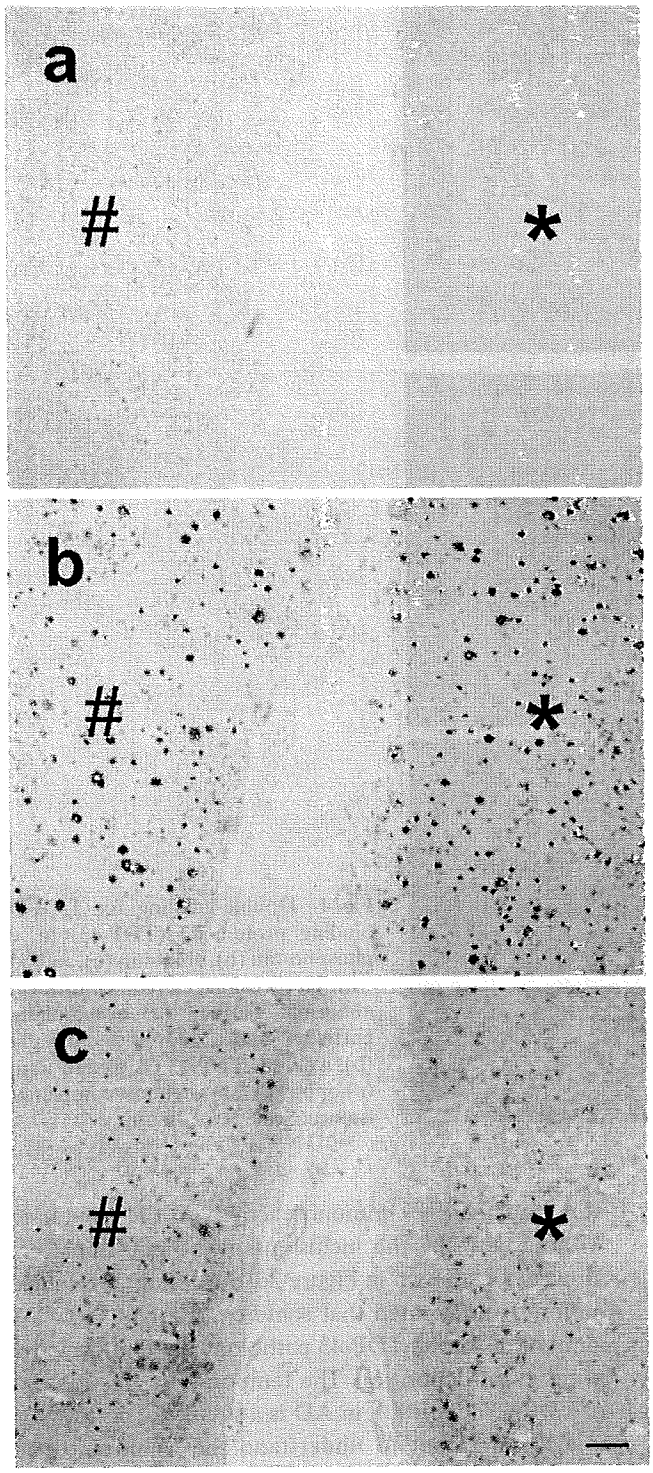

Fig. 3 Topographical distributions of TAR-DNA-binding protein 43 (TDP-43), antibodies against amyloid β (6E10), and AT8 immunoreactivities in serial sections. Whereas abnormal TDP-43 immunoreactivity is restricted in the parahippocampal gyrus (#) in this case (a), 6E10 (b) and AT8 (c) labelings are distributed both in the parahippocampal (#) and occipitotemporal (*) gyri. Scale bar: 100 μm.

immunoreactivity was relatively scarce. However, as shown in Figure 4a–c, some of the TDP-43-positive inclusions were also labeled with anti-AT8 antibody, although the incidence rate was very low.

Because in FTLD-U, TDP-43-positive inclusions were ubiquitinated, a colocalization rate of intraneuronal TDP-43 and ubiquitin was also examined. To carry out this experiment we examined only evident inclusions (not crystal-like shape) that were relatively large (over 5 μm in diameter) because we were afraid of counting artificial stainings. As shown in Figure 4d–f, abnormal TDP-43 inclusions were highly colocalized with ubiquitin (93.5%). Interestingly, TDP-43-positive inclusions were also highly colocalized with the ubiquitin binding protein, p62 (97.5%; Fig. 4g–i).

Finally, the TDP-43 immunoreactivity in cortices other than the hippocampal area was examined. All the medial temporal TDP-43-positive cases also demonstrated the immunoreactivity in the frontal (Fig. 5) but never in the parietal and occipital cortices (data not shown). TDP-43 was also deposited as neuronal intracytoplasmic inclusions (Fig. 5b) and distributed along cortical layers (Fig. 5a,c,d). As shown in Figure 5, the intensity of the TDP-43 immunoreactivity was relatively high.

DISCUSSION

In this study, TDP-43 pathology was detected in 31% of our clinically and neuropathologically typical AD cases. This percentage is in accordance with the results of previous reports describing TDP-43 pathology in 20–34% of AD cases.[13–16] Thus, it is certain that a constant percentage of AD patients show TDP-43 deposition in their brains, and this fact might suggest that AD pathology and TDP-43 proteinopathy have some links in their disease mechanisms. Besides, these percentages were calculated on the basis of TDP-43-positive cases in the hippocampal formation; however, a very recent report demonstrated that a small number of AD cases showed TDP-43-positive inclusions only in the amygdala, and not in the hippocampus.[22] Thus, it is reasonable to assume that the practical emergence rate of TDP-43-positive inclusions in AD might be higher.

The dentate gyrus is the most frequent area where TDP-43-deposits at high density in FTLD-U.[1,16] In AD, Amador-Ortiz *et al.* also showed that all the TDP-43-positive cases demonstrated TDP-43 deposition in the dentate fascia, but their density was not reported.[14] In our study, the topographical distribution of TDP-43 immunoreactivity in the limbic area showed that the inclusions were located in the subiculum and entorhinal cortex at high rates but very rarely in the dentate granule neurons. Higashi *et al.* also described one abnormal TDP-43-positive AD case showing